



**HAL**  
open science

## Characterizing the channel dependence of vegetation effects on microwave emissions from soils

Jiaqi Zhang, Tianjie Zhao, Shurun Tan, Nemesio Rodriguez-Fernandez, Huazhu Xue, Na Yang, Yann Kerr, Jiancheng Shi

► **To cite this version:**

Jiaqi Zhang, Tianjie Zhao, Shurun Tan, Nemesio Rodriguez-Fernandez, Huazhu Xue, et al.. Characterizing the channel dependence of vegetation effects on microwave emissions from soils. *Geo-spatial Information Science*, 2023, pp.1-17. 10.1080/10095020.2023.2275616 . hal-04388755

**HAL Id: hal-04388755**

**<https://hal.science/hal-04388755>**

Submitted on 11 Jan 2024

**HAL** is a multi-disciplinary open access archive for the deposit and dissemination of scientific research documents, whether they are published or not. The documents may come from teaching and research institutions in France or abroad, or from public or private research centers.

L'archive ouverte pluridisciplinaire **HAL**, est destinée au dépôt et à la diffusion de documents scientifiques de niveau recherche, publiés ou non, émanant des établissements d'enseignement et de recherche français ou étrangers, des laboratoires publics ou privés.



Distributed under a Creative Commons Attribution 4.0 International License

# Characterizing the channel dependence of vegetation effects on microwave emissions from soils

Jiaqi Zhang <sup>a,b</sup>, Tianjie Zhao <sup>b</sup>, Shurun Tan <sup>c</sup>, Nemesio Rodriguez-Fernandez <sup>d</sup>, Huazhu Xue <sup>a</sup>, Na Yang <sup>a</sup>, Yann Kerr <sup>d</sup> and Jiancheng Shi <sup>e</sup>

<sup>a</sup>School of Surveying and Land Information Engineering, Henan Polytechnic University, Jiaozuo, China; <sup>b</sup>Aerospace Information Research Institute, Chinese Academy of Sciences, Beijing, China; <sup>c</sup>Zhejiang University/University of Illinois at Urbana-Champaign (ZJU-UIUC) Institute, Zhejiang University, Haining, China; <sup>d</sup>Centre d'Etudes Spatiales de la Biosphère (CESBIO), Université de Toulouse (CNES/CNRS/INRAE/IRD/UPS), Toulouse, France; <sup>e</sup>National Space Science Center, Chinese Academy of Sciences, Beijing, China

## ABSTRACT

The two vegetation transfer parameters of  $\tau$  (Vegetation Optical Depth, VOD) and  $\omega$  (Omega) could vary significantly across microwave channels in terms of frequencies, polarizations, and incidence angles, and their channel-dependent characteristics have not yet been fully investigated. In this study, we investigate the channel dependence of vegetation effects on microwave emissions from soils using a higher-order vegetation radiative transfer model of Tor Vergata. Corn was selected as the subject of investigation, and a corn growth model was developed utilizing field data collected from the multifrequency and multi-angular ground-based microwave radiation experiment from the Soil Moisture Experiment in the Luan River (SMELR). Upon compilation of the simulation dataset of microwave emissions of the corn field, the effective scattering albedo across different channels were calculated using the Tor Vergata model. Results show that vertical polarization of the vegetation optical depth is more affected by incidence angle changes, while horizontal polarization exhibits lower variations in vegetation optical depth due to incidence angle adjustments. The channel dependence of vegetation optical depth can be described as the polarization dependence parameter ( $C_p$ ) and the frequency dependence parameter ( $C_f$ ). These two parameters enable the calculation of vegetation optical depth at any channel under three adjacent frequencies (L-band, C-band and X-band). The effective scattering albedo of vegetation does not vary significantly with vegetation height or angle. It primarily depends on frequency and polarization, showing an overall increasing trend with increasing frequency. The effective scattering albedo with vertical polarization is slightly higher than that with horizontal polarization at higher frequencies, while both are lower in the L-band. This investigation is helpful for understanding the vegetation effects on microwave emissions from soils, ultimately advancing the accuracy of large-scale soil moisture retrieval in vegetated areas.

## ARTICLE HISTORY

Received 14 March 2023  
Accepted 20 October 2023

## KEYWORDS


Vegetation Optical Depth (VOD); effective scattering albedo; vegetation water content; biomass; Tau-omega; Tor Vergata

## 1. Introduction

In addition to being crucial to the surface water, energy, and carbon cycles, the temporal and spatial variability of soil moisture is a major contributor to and indicator of climate change. The majority of the Earth's surface is also covered in vegetation, which has a significant impact on the water cycle, carbon cycle, and surface energy balance (Gentine et al. 2019; Natsagdorj et al. 2017; Pampaloni and Paloscia 1986). Through canopy radiative transfer and photosynthesis, vegetation affects the global carbon cycle and the distribution of surface energy. The processes of canopy radiation transmission and photosynthesis are crucial parts of the physical and biochemical processes in the land surface model, which is an important tool for studying land surface dynamics. While passive microwave remote sensing is a well-established

technology for monitoring soil moisture changes at a large scale, its effectiveness in vegetated areas is reduced. This reduction is due to the scattering and attenuation of soil microwave signals by the vegetation layer, as well as the contribution of the vegetation layer to microwave radiation. As a result, the radiometer's ability to detect soil moisture based on brightness temperature measurements is compromised in such areas. One of the ongoing difficulties in the microwave retrieval of soil moisture is an accurate correction for the effects of vegetation scattering and absorption over a variety of vegetation canopies (Kurum 2013).

Numerous variables, including the texture of bare soil and the soil's dielectric constant, have an impact on the emissivity of soil in vegetated areas. The sensitivity to soil moisture starts to significantly decrease as vegetation density rises. In order to retrieve soil

**CONTACT** Tianjie Zhao  zhaotj@aircas.ac.cn

moisture and establish a connection between ground parameters and microwave observations, it is essential to develop an accurate model. Several models have been developed for this purpose, including the zero-order model (Mo et al. 1982), the first-order model (Ulaby 1982), and the higher-order radiative transfer model (Bracaglia, Ferrazzoli, and Guerriero 1995; Ferrazzoli and Guerriero 1996), among others. The zero-order radiative transfer model typically treats the vegetation canopy as a homogeneous and continuous medium. Due to its straightforward design, the zero-order radiative transfer model is suitable for easy inversion and can be analytically solved with additional assumptions (Zhao et al. 2021). However, studies reveal that when the interior volume scattering is ignored, the total emissivity is usually underestimated and is only appropriate for low-frequency or sparse vegetation (Cheng, Huang, and Gong 2015; Park et al. 2020). As the frequency increases, the first-order volume scattering becomes more pronounced. The extension of the zero-order model to higher frequencies and higher biomass areas has generated great interest in the scientific community.

Indeed, to gain a comprehensive understanding of the impact of vegetation on passive microwave radiation signals, it is necessary to consider the multiple scattering effects generated by components such as leaves and branches within the vegetation canopy. These components contribute to the overall scattering process and can significantly influence the observed microwave signals. Using a geometric and physical approximation, Ferrazzoli and Guerriero devised a discrete passive microwave radiation transfer model in 1996 to simulate the brightness temperature of plants at different frequencies (Ferrazzoli and Guerriero 1996). Several similar thin sub-layers of the vegetation canopy are continuously stacked. The radiative transfer process, which has been confirmed in prior research, completely takes into account the scattering process inside the vegetation canopy. With good findings from both model estimates and radiometer observations, Ferrazzoli and Guerriero in 1996 analyzed forest brightness temperature data obtained at seven distinct bands in Switzerland, ranging from 1.5 GHz to 11 GHz. The simulated emissivity of the Tor Vergata model and the emissivity determined by Della Vecchia et al. using the airborne L-band data of Les Landes data are likewise in good agreement (Della Vecchia et al. 2007). Zhang et al. tested the applicability of the Tor Vergata model in low transmissivity areas by studying the relationship between emissivity, transmissivity, and biomass under dense vegetation (Zhang et al. 2014). In addition, this approach performs well in other passive microwave applications, such as simulating microwave radiation signals from dry snow with high

volume scattering (Jiang et al. 2007). Somayeh evaluated and calculated the Microwave Vegetation Index (MVI) model in 2019 using the brightness temperature approximated by the Tor Vergata model, and she also provided additional suggestions for upcoming satellite and algorithm development using MVI (Talebiesfandarani et al. 2019).

Most of the current soil moisture retrieval algorithms are based on the zero-order model, which directly obtains the parameters related to the physical characteristics of vegetation through the empirical relationship (Kurum 2013). In the zero-order model, vegetation is regarded as a uniform medium, and the multiple scattering effect of electromagnetic waves passing through the medium layer is ignored (Fung et al. 1994). The model divides the total brightness temperature into three parts: the brightness temperature contributed by vegetation, the brightness temperature contributed by the soil layer after the scattering and attenuation of the vegetation, and the brightness temperature contributed by the interaction between the vegetation and soil. If we want to calculate the total brightness temperature accurately, accurate  $\tau$  and  $\omega$  are indispensable. Due to the complexity of surface vegetation types,  $\tau$  and  $\omega$  differ greatly under different microwave frequencies, polarizations, and incidence angles, which will greatly affect the calculated brightness temperature of vegetated areas (Wigneron et al. 2003). Due to the differences in vegetation optical depth and single scattering albedo at different channels, quantifying channel-dependent parameters can calculate radiative characteristic parameters more accurately in unknown channels, thus improving the retrieval accuracy of the zero-order radiative transfer model.

The accurate accounting of multiple scattering effects in vegetation on passive microwave radiation signals is a critical challenge. Developing more precise models that consider the scattering process inside the vegetation canopy is essential for better estimating the brightness temperature of plants at different frequencies. To improve the accuracy of soil moisture retrieval in vegetated areas, the parameters of the zero-order  $\tau$ - $\omega$  model need to be optimized.

In this study, the model of corn crop growth under different environmental conditions and vegetation properties was employed to establish an input database. The Tor Vergata model was then substituted to simulate microwave emissions from corn-covered soil. The simulations generated by the Tor Vergata model were used to optimize the model parameters of the zero-order  $\tau$ - $\omega$  model. Furthermore, the analysis of the dependence of the vegetation effects on the frequency, polarization, and incidence angle was carried out, considering vegetation optical depth and effective scattering albedo.

## 2. Experimental data

The site (42.18°N, 116.47°E) of the multifrequency and multiangle ground-based microwave radiation observation experiment was located in the Luan River basin (Zhao, Shi et al. 2020). In this study, the dataset served as a validation set for the accuracy of the Tor Vergata model. This dataset includes the brightness temperature data, soil data, and vegetation data (Zhao, Hu et al. 2020, 2021). The experimental site has taken into account the effects of soil moisture, soil properties, soil roughness, and planting density on the experimental results. Additionally, data processing has been done in a way that aims to achieve as much uniformity as possible. Therefore, it is considered that the influence of heterogeneity on brightness temperature can be ignored.

### 2.1. Microwave radiometry

The vehicle-mounted dual-polarized multi-frequency radiometer (RPG-6CH-DP) used in this study contains three frequencies: L-band (1.41 GHz), C-band (6.925 GHz) and X-band (10.65 GHz). The L-band works with a planar patch array, and the C- and X-bands share a parabolic antenna (configurations shown in Table 1). All three bands (six channels) can work simultaneously to obtain dual-polarized multi-frequency brightness temperatures.

### 2.2 Soil properties and surface roughness

The soil moisture (Figure 1) and temperature were simultaneously measured by Decagon EM50 data

**Table 1.** The specifications of the RPG-6CH-DP radiometer.

| Parameter              | L-band                             | C-band            | X-band    |
|------------------------|------------------------------------|-------------------|-----------|
| Frequency              | 1.41 GHz                           | 6.925 GHz         | 10.65 GHz |
| Bandwidth              | 20 MHz                             | 400 MHz           | 400 MHz   |
| Geometry               | Planar 64 square patch array       | Parabolic antenna |           |
| Half power beam width  | 11°                                | 6.85°             | 6.11°     |
| Side lobe level        | < -30 dB                           | < -30 dB          | < -35 dB  |
| Radiometric resolution | <0.2 K @ 1 second integration time |                   |           |

loggers with 5TM probes every 10 min. The nominal resolution and accuracy of the 5TM probe are  $0.0008 \text{ cm}^3/\text{cm}^3$  ( $\pm 0.03 \text{ cm}^3/\text{cm}^3$ ) for soil moisture and  $0.1 \text{ K}$  ( $\pm 1 \text{ K}$ ) for soil temperature. Soil moisture and temperature were measured at depths of 2.5 cm, 10 cm, 20 cm, 30 cm and 50 cm. The soil texture was measured in the laboratory, and it was found that the field consists of loamy sand with a sand fraction of 80% and a clay fraction of 10%

The soil surface roughness may lead to different effects on the microwave observations in terms of the frequency, polarization and incidence angle used (Anderson et al. 2004). The surface roughness was measured by taking pictures of a 1-m needle board, and the root mean squared height,  $s$ , and correlation length,  $l$ , were calculated after digitalizing the surface height profile. Measurements were taken in both the north–south direction and east–west direction over the field. The surface roughness did not vary greatly during the experimental period, with average values of  $s = 0.82 \text{ cm}$  and  $l = 12.21 \text{ cm}$  for the corn field.

### 2.3 Vegetation properties

During the growth of crops, the vegetation contribution of the microwave radiation is becoming increasingly important. Measurements of vegetation properties, including the vegetation water content, Leaf Area Index (LAI), the half-leaf length, thickness, and density of leaves and the radius, length, and density of branches., were conducted manually on selected days. The vegetation water content was measured by using a destructive sampling method (the fresh and dry weights), with the leaf and stem water contents measured separately. Crop LAI was obtained with destructive vegetation samples by digital photograph analysis. The plant height was acquired with a measuring tape. Geometric parameters include the leaf radius and thickness. Occasionally, a leaf is not in the shape of a standard disc; thus, a smaller disk with the same half leaf length is used to simulate the leaf radius. Moreover, the stem length was also measured during the experiment.

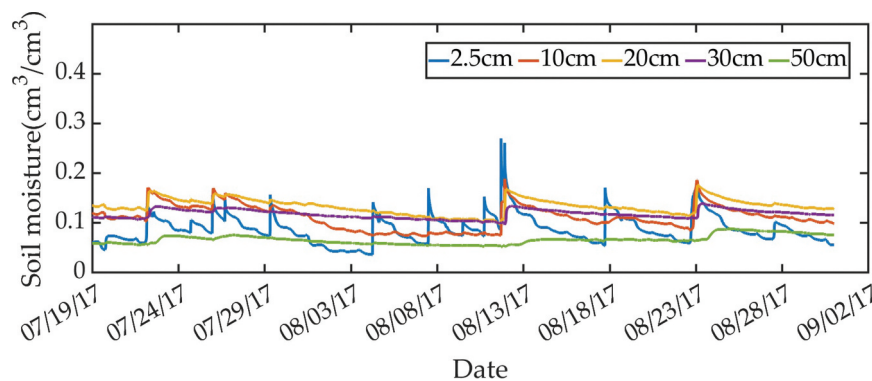


**Figure 1.** Soil moisture data.

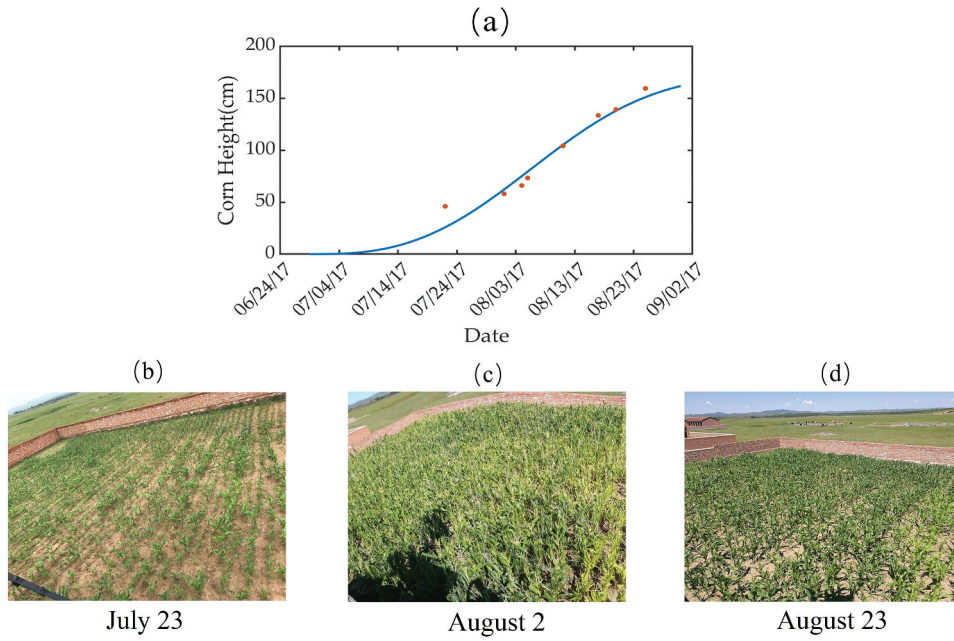


**Figure 2.** (a) Measurements of height. Dots show the measured values, and solid lines are the fitted functional relationships. (b) photography on July 23, 2017, (c) photography on August 2, 2017, and (d) photography on August 23, 2017.

A square plot of 25 m by 15 m was planted with corn, and the brightness temperature data were routinely recorded from 19 July 2017, to 30 August 2017, with the exception of a radiometer storage malfunction that caused data collection to be suspended between August 11 and August 17. The multifrequency and multi-angle brightness temperatures of corn, as well as associated soil and vegetation data, are covered. These data are crucial for modeling and verifying surface microwave radiation as well as developing and testing soil moisture retrieval algorithms.

### 3. Methodology

#### 3.1. Crop growth model of corn

Simulations of microwave emissions from land surfaces are challenging to perform due to the complexity of soil and vegetation properties. In terms of the soil parameters, the soil texture, soil moisture, and soil surface roughness (correlation length and root mean squared height) can influence microwave emissions. Regarding vegetation, the total microwave emission can be affected by branches, leaves, trunks and their size, density and water content. To simulate the various scenarios during vegetation growth, a crop growth model for corn with a large number of dynamic parameters was used in this study.

During the Soil Moisture Experiment in the Luan River (SMELR), vegetation parameters were measured by destructive sampling. Since the vegetation water content ( $\text{kg}/\text{m}^2$ ) measurements are discontinuous, we need to construct a continuously changing dataset for the subsequent analysis. Here, we used a two-variable linear model in which the vegetation water content is the sum of the water content of its leafy parts and stem parts:

$$WVC = VWC_{\text{leaf}} + VWC_{\text{stem}} = A \cdot LAI + B \cdot hgt \quad (1)$$

where  $VWC$  is the vegetation water content;  $A \cdot LAI$  is the leaf water content  $VWC_{\text{leaf}}$ ; and  $B \cdot hgt$  accounts for the stem water content  $VWC_{\text{stem}}$ .

It is assumed that there is also a linear relationship between LAI and vegetation height  $hgt$  (Byrne, Kiely, and Leahy 2005; Della Vecchia et al. 2006), according to previous studies. The slope is approximated by the ratio between the maximum LAI ( $LAI_{\text{max}}$ ) and the maximum vegetation height ( $hgt_{\text{max}}$ ).

$$LAI = \frac{LAI_{\text{max}}}{hgt_{\text{max}}} \cdot hgt \quad (2)$$

A simple “S”-shaped growth model was then used to predict the vegetation height as a function of time Figure 2(a):

$$hgt = hgt_{\text{max}} \cdot (1 - \exp(-k \cdot t^b)) \quad (3)$$

where  $k$  and  $b$  are fitted coefficients; and  $t$  is the time in days, counting from the day of sprouting (29 June 2017). Figure 2(a) shows the fitting results of the measured vegetation water content with the daily values from the dataset. Figures 2(b-d) illustrate the growth stages of corn in the experimental field as it varies with time.

This growth model is mostly based on the measured data discussed in the previous section. The crop growth model of corn uses the height of the vegetation as the primary variable parameter to calculate the physical properties of the corn leaf, petiole, and trunk.

Firstly, due to the non-linear nature of corn development, different parts of the plant will exhibit varying growth rates at different stages of the growth cycle.

Studies have revealed a large dynamic range of brightness temperature from the sowing to the maturity stages, and a strong relationship of brightness temperature with biomass and height (Dela Torre, Gao, and Macinnis-Ng 2021). In this model, the plant height of corn is used as the main parameter. For example, the vertical stem parameters are directly related to plant heights, and the specific equation is expressed as follows:

$$h_{\text{stalk}} = 0.75 \times hgt \quad (4)$$

$$r_{\text{stalk}} = \begin{cases} hgt \div 50, & hgt \leq 50 \\ 1 + 0.75 \times (hgt - 50) \div 150, & 50 < hgt \leq 200 \end{cases} \quad (5)$$

where  $h_{\text{stalk}}$  (cm) is the height of the corn stalk,  $hgt$  (cm) is the total height of the corn plant, and  $r_{\text{stalk}}$  (cm) is the radius of the corn stalk. The growth rate of the stem radius is slightly slower than that of the flowering spike stage when the height of corn vegetation is less than 50 cm. It was found that the corn stalk diameter increases as the plant grows up to maximum value of 1.75 cm.

The canopy of corn is primarily characterized by the single leaf area, which serves as an indicator of the canopy scatterer parameter. Before the maturity stage, corn leaves and petioles continue to grow constantly, but once the maturity stage has passed and more corn nutrition has been directed into the development of corn grains, the fundamental growth range of the corn leaves and petioles is much smaller. The specific performance equation of the canopy scatterer parameters is as follows:

$$S_{\text{leaf}} = \begin{cases} 150 \times hgt \div 50, & hgt \leq 50 \\ 150 + 250 \times (hgt - 50) \div 150, & 50 < hgt \leq 200 \end{cases} \quad (6)$$

$$r_{\text{leaf}} = \sqrt{\frac{S_{\text{leaf}}}{8 \times \pi}} \quad (7)$$

$$r_{\text{petiole}} = r_{\text{max}} \times \sqrt[4]{(S_{\text{leaf}} \div 400)} \quad (8)$$

where  $S_{\text{leaf}}$  is the single leaf area,  $r_{\text{leaf}}$  is the radius of the small disk, and  $r_{\text{petiole}}$  is the radius of the small cylinder of the petiole. The leaf density was then determined using LAI from the dataset.

If we want to generate a comprehensive vegetation radiative transfer characteristics database, we must additionally establish the soil conditions, with the soil moisture change set to 2%-30% and the step size set to 2%. This occurs after the vegetation parameters are specified. The soil roughness root mean square error is set to 0.8 cm–1.2 cm, the step size is 0.2 cm, the surface roughness correlation length is set to 9 cm–12 cm, and the step size is 1 cm because the soil roughness conditions are also fairly varied. The Tor Vergata

model was used to simulate parameters including the total emissivity, transmissivity, and bare soil emissivity when the above parameter sets were complete, and a corresponding database was created.

### 3.2. Radiative transfer model of the vegetated surface

#### 3.2.1 Tor vergata model

The Tor Vergata model is a higher-order radiative transfer model based on the matrix doubling algorithm that models the physical interactions between electromagnetic waves and vegetation as discrete scatterers. The model divides the vegetation layer into multiple thin sublayers and calculates the scattering matrix of the entire plant layer using the matrix doubling algorithm. The emissivity of the whole vegetation layer is then determined through energy conservation calculations. The model includes three layers: the canopy layer, trunk layer, and soil layer.

The Tor Vergata model uses electromagnetic waves and geometric approximations to model the scatterers in the canopy layer. In Figure 3(a), small discs represent leaves, and small cylinders represent branches or petioles, with the number of discs calculated based on the LAI and leaf width. For plants like corn with broad leaves and a certain curvature, using a leaf model that better fits the curvature of vegetation leaves is more appropriate because it can better capture the complex geometric shape and orientation of corn leaves (Della Vecchia et al. 2006). However, in the design process of multi-frequency and multi-angle ground-based observation experiments, more emphasis was placed on the variations of simple shape parameters during vegetation growth, and detailed leaf curvature data were missing. Therefore, the traditional approach of modeling with small discs was ultimately adopted (Monsivais-Huertero and Judge 2010; Monsivais-Huertero, Liu, and Judge 2018; Stiles, Sarabandi, and Ulaby 2000).

The scattering phase matrix and extinction vector for disks and cylinders are calculated using the Rayleigh approximation at low frequencies (Eom and Fung 1984, 1986; Osborn 1945), and the physical optical approximation is used for disks at frequencies higher than 5 GHz (Levine et al. 1983). For small cylinders, an infinite length approximation is used to represent the inner field (Karam and Fung 1988). The scatter matrix  $\mathbf{S}$  of the scatterer was calculated after obtaining the Bistatic scattering cross section through the above simulations.

$$S_{ijpq0} = \int_0^{2\pi} \frac{n\Delta z\Delta\theta \sin\theta_j}{4\pi \cos\theta_{si}} \sigma_{ijpq}(\Phi_s - \Phi) d(\Phi_s - \Phi) \quad (9)$$

where  $\sigma_{ijpq}(\Phi_s - \Phi)$  is the bistatic scattering cross section averaged among  $\theta_j$  and  $\theta_{si}$  belonging to the  $j$ -th and  $i$ -th intervals of the upper half space,

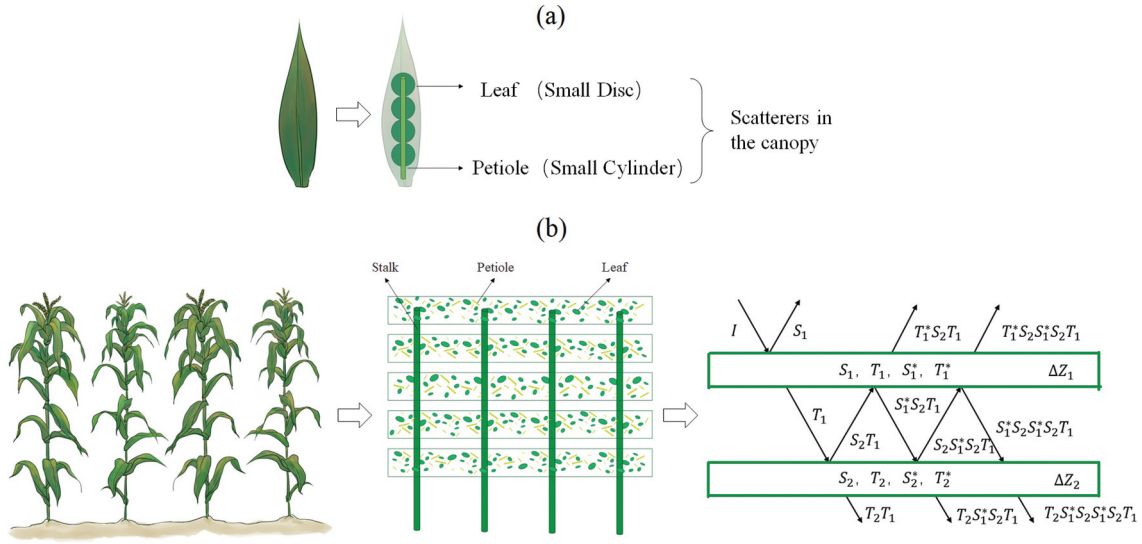


**Figure 3.** (a) scatterer representation of corn leaves in the model. (b) Tor Vergata model structure and matrix doubling algorithm diagram.

respectively. Moreover,  $p$  and  $q$  are the scattering and incidence polarizations, respectively. Similarly, the elements of the  $T$  matrix can be computed by:

$$T_{ijpq0} = \int_0^{2\pi} \frac{n\Delta z \Delta \theta \sin \theta_j}{4\pi \cos \theta_{si}} \sigma'_{ijpq}(\Phi_s - \Phi) d(\Phi_s - \Phi) \quad (10)$$

where  $\sigma'_{ijpq}(\Phi_s - \Phi)$  is the bistatic scattering cross section averaged among  $\theta_j$  and  $\theta_{si}$  belonging to the  $j$ -th and  $i$ -th intervals of the upper half space, respectively.

In Figure 3(b), the core of the matrix doubling algorithm is to assign these scatterers to each sublayer and then use the lower hemisphere scatter matrix  $T$  and the upper hemisphere scatter matrix  $S$  to merge the two adjacent thin sublayers. The specific equation is as follows:

$$\begin{aligned} S &= S_1 + T_1^* S_2 T_1 + T_1^* S_2 S_1^* S_2 T_1 + \dots \\ &= S_1 + T_1^* S_2 (1 - S_1^* S_2)^{-1} T_1 \end{aligned} \quad (11)$$

$$\begin{aligned} T &= T_2 \left[ 1 + S_1^* S_2 + (S_1^* S_2)^2 + \dots \right] T_1 \\ &= T_2 (1 - S_1^* S_2)^{-1} T_1 \end{aligned} \quad (12)$$

In Equations (11) and (12),  $S_1$  and  $S_2$  represent the upper hemisphere scatter matrix of Incident Sublayer 1 and Incident Sublayer 2 from above, respectively. After reversing the incidence angle, the scattering matrix is represented by the superscript  $*$ . In the process of dividing the vegetation canopy into thin layers, the thickness of each thin layer is denoted as  $\Delta z_1$ . Respectively, combining the sublayers  $\Delta z_1$  and  $\Delta z_2$  into a new thicker sublayer  $\Delta z$  ( $\Delta z = \Delta z_1 + \Delta z_2$ ), then repeating this combination  $N$  times, the scattering matrix of the full canopy can be obtained.

The Tor Vergata model uses an infinite length approximation to represent the trunk layer and the Integral Equation Model (IEM) to represent the soil layer. The input parameters for the soil layer include the soil roughness height standard, soil roughness correlation length, and soil moisture. The scattering matrix of the vegetation-soil layer is calculated by using the Matrix Doubling algorithm to double the vegetation layer and soil layer scattering matrix, obtained by first calculating the scattering matrix and transmission matrix for the entire canopy layer and then using the soil layer scattering matrix calculated using IEM. The total scattering matrix  $S_T$  is:

$$S_T = S_{\text{veg}} + T_{\text{veg}}^* S_{\text{soil}} (1 - S_{\text{veg}}^* S_{\text{soil}})^{-1} T_{\text{veg}} \quad (13)$$

The subscripts veg and soil represent the vegetation layer and soil layer, respectively, and the emissivity contributed by each component can be calculated by integrating the upper half space. The equation is as follows:

$$e_{jiq} = 1 - \sum_{i=1}^{N_\theta} \sum_{p=1}^2 \frac{\cos \theta_{si} \sin \theta_{si}}{\cos \theta_j \sin \theta_j} S_{Tijpq} \quad (14)$$

The brightness temperature ( $T_B$ ) of the vegetation may be determined from the total emissivity of the vegetation if the actual temperature  $T_{\text{veg}}$  of the vegetation is known. The equation reads as follows:

$$T_{Bjiq} = e_{jq} \times T_{\text{veg}} \quad (15)$$

### 3.2.2 Tau-Omega model

The zero-order model, which is a semiempirical model based on radiative transfer theory, is commonly used in conventional soil moisture retrieval algorithms. The

total brightness temperature ( $T_B$ ) can be calculated using the following equation:

$$\begin{aligned} T_{B_{P,\theta,f}}^{total} = & T_{veg} \cdot (1 - \omega_{P,\theta,f}) \cdot (1 - \Gamma_{P,\theta,f}) \\ & + T_{veg} \cdot (1 - \omega_{P,\theta,f}) \cdot (1 - \Gamma_{P,\theta,f}) \\ & \cdot \gamma_{P,\theta,f}^{soil} \cdot \Gamma_{P,\theta,f} + T_{soil} \cdot (1 - \gamma_{P,\theta,f}^{soil}) \cdot \Gamma_{P,\theta,f} \end{aligned} \quad (16)$$

The microwave radiometer received signal during the passive microwave remote sensing of vegetation is composed of three components, as described by Equation (16).  $T_{veg} \cdot (1 - \omega_{P,\theta,f}) \cdot (1 - \Gamma_{P,\theta,f})$  represents the radiation contributed by the vegetation layer, where  $T_{veg}$  is the actual temperature of the vegetation,  $\omega$  is the scattering albedo, and  $\tau$  is the vegetation optical depth.  $T_{veg} \cdot (1 - \omega_{P,\theta,f}) \cdot (1 - \Gamma_{P,\theta,f}) \cdot \gamma_{P,\theta,f}^{soil} \cdot \Gamma_{P,\theta,f}$  represents downwelling and reflected from the vegetation, where  $\gamma_{P,\theta,f}^{soil}$  is the reflectivity of the surface.  $T_{soil} \cdot (1 - \gamma_{P,\theta,f}^{soil}) \cdot \Gamma_{P,\theta,f}$  represents the radiation scattered by the vegetation onto bare soil. To accurately explain the microwave radiation characteristics of vegetation, accurate bare soil data and plant parameters are needed. The  $\tau$ - $\omega$  model is widely used in soil moisture retrieval algorithms due to its simplicity and commonly required parameters. However, from a theoretical perspective, the  $\tau$ - $\omega$  model is not as accurate in areas with dense vegetation and scatterers since these scatterers are large in relation to the wavelength and require the application of a higher-order model to account for scattering within the vegetation. By applying the  $\tau$ - $\omega$  model and maintaining the model's basic structure, more precise vegetation optical depth and scattering albedo may more effectively explain the multiple scattering effects of vegetation and simulate the scattering properties of the vegetation canopy.

### 3.3. Vegetation optical depth

The  $\tau$ - $\omega$  model considers the vegetation layer as a homogeneous and continuous interference medium during the transmission of vegetative radiation. This model is widely used in large-scale soil moisture retrievals due to its simple structure. The scattering albedo and vegetation optical depth are two essential inputs for the model. The Tor Vergata model uses the vegetation input parameters for different frequency bands, such as the scattering albedo and vegetation optical depth, to compute the scattering matrix and extinction vector of disks and cylinders using the Rayleigh-Gans approximation and physical optical approximation. The number of thin sublayers and the extinction vector equation can be used to determine the canopy transmissivity, which is expressed as:

$$\Gamma_{veg} = (e^{-k_{el} - k_{eb}})^n \quad (17)$$

where  $k_{el}$  is the extinction vector of small discs in each thin sublayer,  $k_{eb}$  is the extinction vector of small cylinders in each thin sublayer, and  $n$  is the number of thin sublayers in the canopy.

Therefore, the vegetation optical depth of the canopy in the Tor Vergata model can be defined as:

$$\Gamma_{P,\theta,f} = \exp(-\tau_{P,\theta,f} \cdot \sec\theta) \quad (18)$$

Since the Gauss–Legendre method is used in the Tor Vergata model, each of them is divided into a range of angles. The direction of the simulated incident angle is also determined by the size of the angular interval because the angular interval is also determined by the real incident angle. As a result, the vegetation's transmissivity will vary depending on the incident angle, which will also have an impact on the vegetations optical depth.

Specific frequency, angle, and polarization dependences apply to the optical depth of vegetation. Therefore, it will be useful for next zero-order models if its dependency can be parameterized or empirically represented. Development is truly beneficial. We use the following equation to represent the vegetation optical depth for any two different channels:

$$\frac{\tau_1}{\tau_2} = \left(\frac{f_1}{f_2}\right)^{C_f} \frac{\sin^2\theta_1 C_{P_1} + \cos^2\theta_1}{\sin^2\theta_2 C_{P_2} + \cos^2\theta_2} \quad (19)$$

where  $C_f$  is the frequency-dependent parameter of vegetation optical depth, and  $C_p$  is the polarization-dependent parameter. At the same time,  $C_f$  and  $C_p$  also have a specific correlation with vegetation types. It has been reported that  $C_f = 0.5$  in Pampaloni and Paloscia (Pampaloni and Paloscia 1986). Jackson and Schmugge reported that  $C_f = 1.08$  for wheat and  $C_f = 1.38$  for soybeans. The “isotropic” case,  $C_p = 1$ , corresponds to the assumption used in this study that the vegetation tau is independent of both the polarization and incidence angle ( $\tau_V = \tau_H = \tau^0$  at nadir), which is a commonly used assumption in previous studies (Fernandez-Moran et al. 2017; Kerr et al. 2012; Wigneron et al. 2004).

### 3.4. Effective scattering albedo

Scattering albedo refers to the proportion of radiation that is scattered during the extinction process. Due to the simple structure of the zero-order radiative transfer model, only single scattering within the vegetation canopy is considered. The higher-order radiative transfer model, which simulates the interactions of scattering bodies within the vegetation and multiple extinction processes, cannot be simply defined as the vegetation single-scattering albedo in order to achieve better simulation results. In this study, an effective scattering albedo is defined as a simplified representation of the scattering effect in the vegetation canopy.



The zero-order radiative transfer model can be optimized by fitting it to the computed emissivity from the Tor Vergata model using a least squares approach:

$$\sigma = \sqrt{\sum_{i=1}^N (e_{1i} - e_{2i})^2} \quad (20)$$

where  $N$  is the number of simulated experiments,  $e_{1i}$  is the total vegetation emissivity calculated by the Tor Vergata model, and  $e_{2i}$  is the total vegetation emissivity calculated by the  $\tau$ - $\omega$  model. The acquired vegetation optical depth, obtained through least-squares fitting, can be utilized to calculate the effective albedo. The integration of the Tor Vergata model and the tau-omega model into the computation allows for a more precise representation of the volume scattering inside vegetation features, improving the accuracy of the brightness temperature modeling for various plant types.

#### 4. Results and discussion

In this study, ground-based multi-frequency, multi-angle microwave radiometer observations were used for model validation and combined with simultaneous observations to develop a corresponding corn growth model. Different channels and different soil conditions were simulated and a database of microwave radiation properties was established using the Tor Vergata model. The Degree of Information (DoI) ensures that no more parameters are retrieved than the information content in the observations allows (Konings et al. 2015).

In the radiometer dataset, the calculated DoI values for various frequencies, angles, and polarizations are as follows: 5.9004 for the L-band, 5.8204 for the C-band, and 5.7280 for the X-band. And in the simulated database, the calculated DoI values are as follows: 13.6538 for the L-band, 13.7483 for the C-band, and 13.3450 for the X-band. Notably, when considering the dual-angle combination, the L-band exhibits a higher DoI compared to the C- and X-bands. This finding suggests that, in a multi-angular configuration, the L-band offers greater sensitivity to overall vegetation and soil moisture, making it an optimal band for soil moisture retrievals. Furthermore, the incorporation of multiple frequencies results in an increased DoI, with the database's overall DoI calculated as 40.5307, indicating sufficient information content for the inversion of omega.

##### 4.1. Validation of the tor vergata model

In this study, the reliability of the Tor Vergata model was evaluated by comparing the simulated brightness temperature with real-world brightness temperature

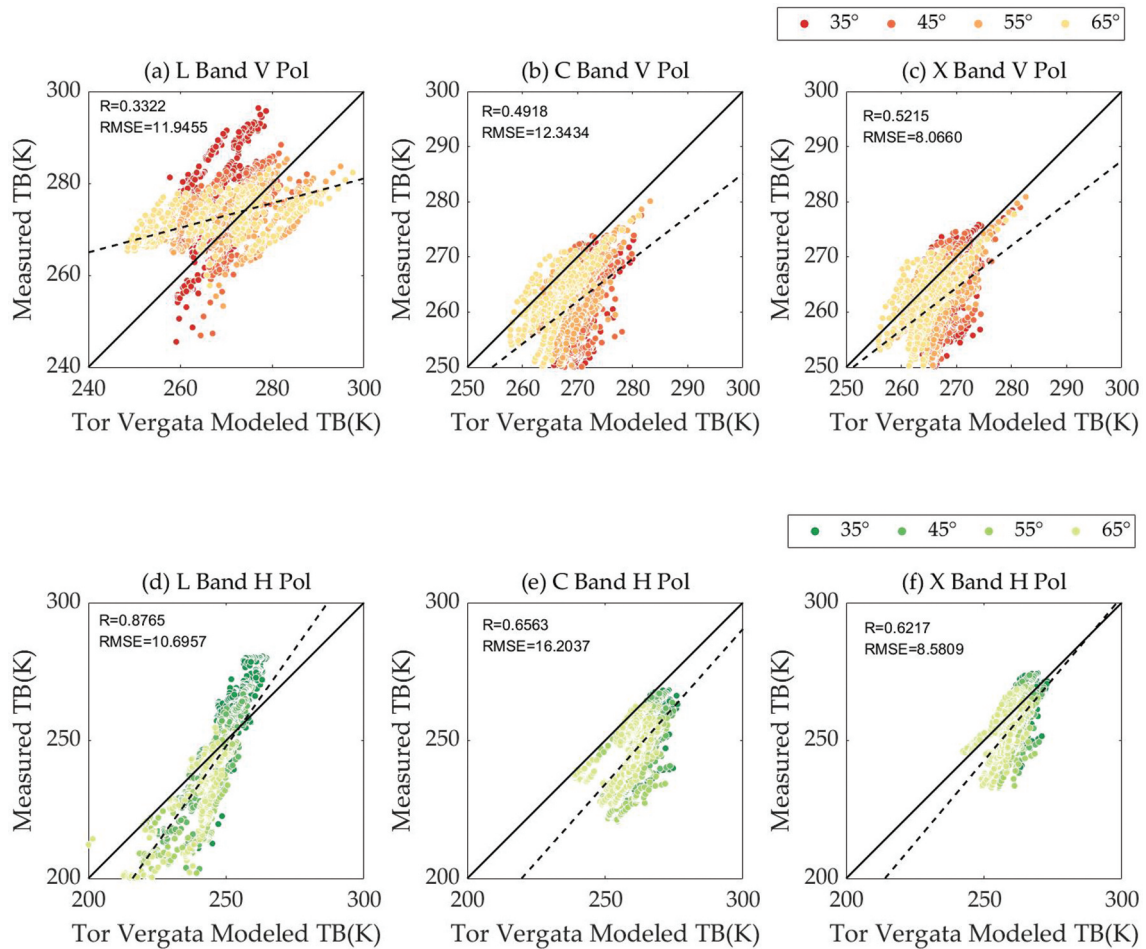
obtained from field observations. The accuracy of the model was assessed using data collected during an experiment that measured ground-based microwave radiation at various frequencies and angles on a corn field. The leaf area index and fitted corn height data were incorporated into the corn growth model, and the vegetation and soil data were input into the Tor Vergata model for brightness temperature simulation.

Figure 4 presents a scatter plot comparing the radiometer-observed brightness temperature with that simulated by the Tor Vergata model between July 19 and August 30 in the dataset under horizontal polarization of the L-band, C-band, and X-band. The results demonstrate that the Tor Vergata model combined with the corn growth model achieves a high verification accuracy in all three bands. The correlation coefficient ( $R$ ) of the simulated results ranges from 0.8765, and the Root Mean Square Error (RMSE) ranges from 8.6K to 16.2K. The validation confirms the high accuracy of the Tor Vergata model. Furthermore, the simulation results of the Tor Vergata model are consistently better for horizontal polarization compared to vertical polarization.

The three components that make up the emissivity in the tau-omega model are the radiation produced by the vegetation layer, the radiation produced by the vegetation layer's downwards reflection through the ground, and the radiation emitted by the vegetation's scattering on the bare ground. Using a corn plant with a height of 200 cm and grown in similar soil conditions, the independent components of the Tor Vergata model can also be computed.

In Figures (5-7), the contribution of each component to the overall emissivity is depicted. The changing trend and contribution degree with the angle are found to be in good agreement with the Tau-Omega and Tor Vergata models in the L-band, with vegetation depicted as the dark green area. The contribution component in the Tau-Omega model's equation is represented by  $(1 - \omega_{p,\theta,f}) \cdot (1 - e^{-\tau_{p,\theta,f} \cdot \sec\theta})$ . The bright green area represents the radiation emitted by plants on bare soil, represented as  $(1 - \gamma_{p,\theta,f}^{\text{soil}}) \cdot e^{-\tau_{p,\theta,f} \cdot \sec\theta}$ , while the vegetation component is denoted by  $e^{-\tau_{p,\theta,f}}$ . As the incidence angle increases, the primary component of the emissivity contribution shifts from soil to vegetation due to the increasing extinction effect of vegetation. As shown in Figure 6, in the C-band, the volume scattering inside the vegetation increases, making vegetation scattering more emissive and rendering the tau-omega model less applicable.

As shown in Figure 7, similar radiative behavior is also observed in the higher frequency X-band. However, as frequency rises and penetration decreases, the extinction impact of vegetation becomes more pronounced, and the influence of the soil's contribution to the scattering and absorption of the



**Figure 4.** Scatter plot comparing soil moisture experiment in the Luan River observations brightness temperature with Tor Vergata model simulations brightness temperature (a) L-band vertical polarization (b) C-band vertical polarization (c) X-band vertical polarization (d) L-band horizontal polarization (e) C-band horizontal polarization (f) X-band horizontal polarization.

microwave passing through the vegetation becomes more evident, resulting in a steady decline in the ground's contribution to emissivity. Although the contributions of its many components can vary greatly, there may not be a noticeable change in the overall emissivity performance.

#### 4.2. Channel dependency of the vegetation optical depth

The transmissivity of corn at various angles, polarizations, and heights was derived from simulations. The results reveal a high degree of regularity in the transmissivity behavior. As the height of the plant canopy increases, the transmissivity decreases gradually due to the growth of leaves and branches, resulting in an increase in the biomass. Additionally, as the incidence angle increases, the path length of the electromagnetic wave through the vegetation increases, leading to a decrease in the transmissivity. The frequency also influences the transmissivity, with the transmissivity decreasing as the frequency increases due to the decrease in the penetration with shorter wavelengths. The relationship between the vegetation optical depth

in the L-band, C-band, and X-band and Vegetation Water Content (VWC) under vertical polarization is shown in Figure 8. A strong linear relationship has been demonstrated between the vegetation optical depth and vegetation water content. The VOD can be estimated using the traditional semiempirical equation,  $\tau = b \cdot VWC$ , where the factor  $b$  is influenced by the frequency and plant structure, with the influence diminishing as the frequency increases. However, it has been shown that the traditional semiempirical model does not fully account for the increase in the vegetation canopy volume scattering signal at high frequencies. The physical model employed by the Tor Vergata model provides a more precise estimate of the VOD compared to the conventional semiempirical technique. As a result, when computing the effective scattering albedo, the VOD estimated by the Tor Vergata model may be used as the true value.

As depicted in Figure 9, the correlation between the vegetation optical depth, incidence angle, and height was determined using the Tor Vergata model for three different wavebands. The model is more accurate and has a stronger physical model foundation than the traditional empirical vegetation optical depth

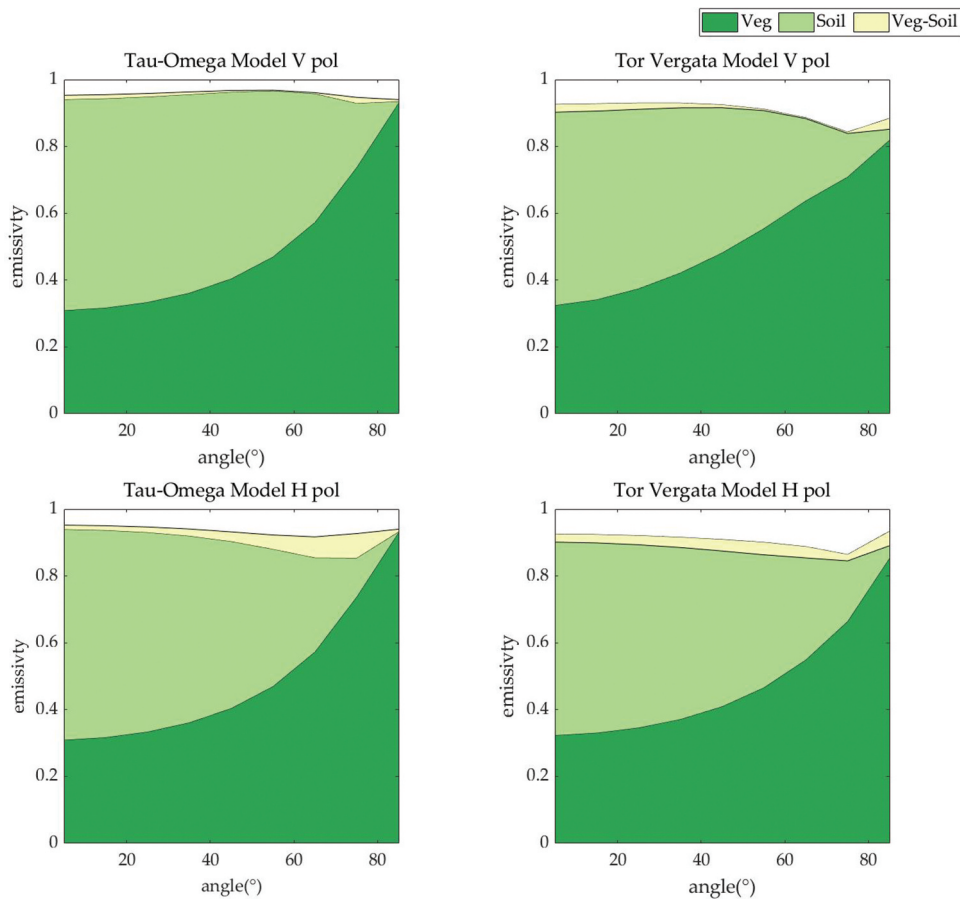


Figure 5. Tau-Omega model and Tor Vergata model brightness temperature composition in the L-band.

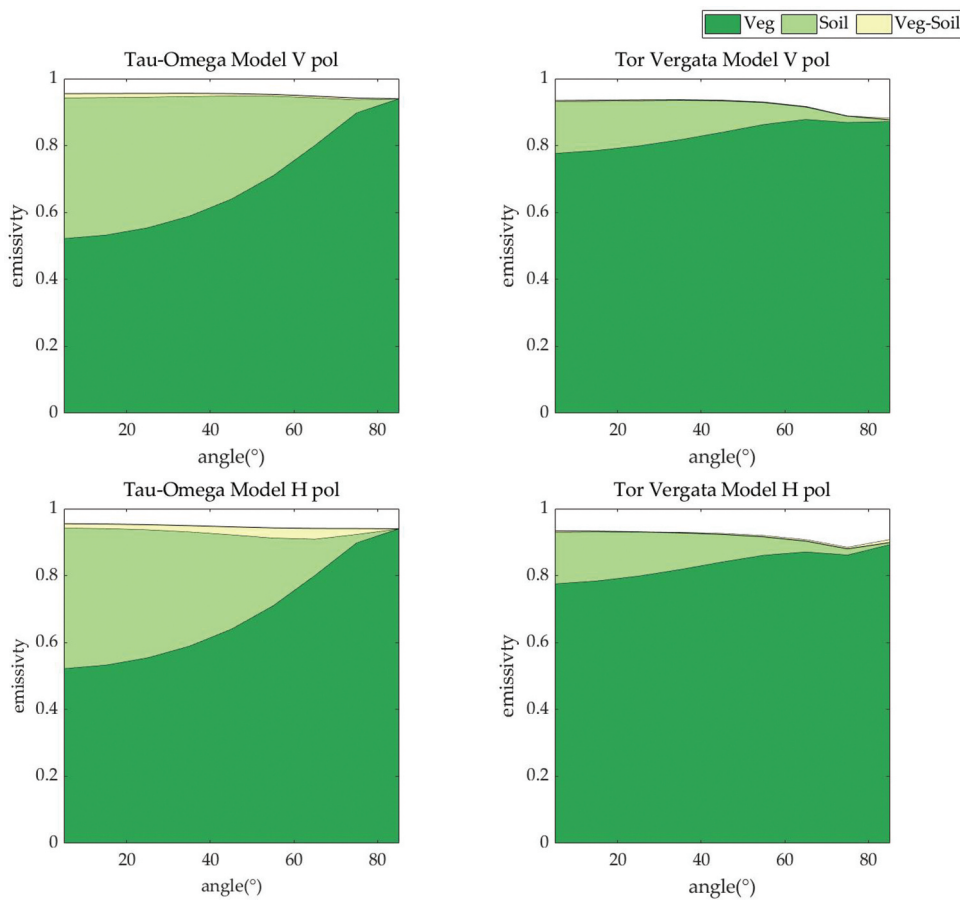
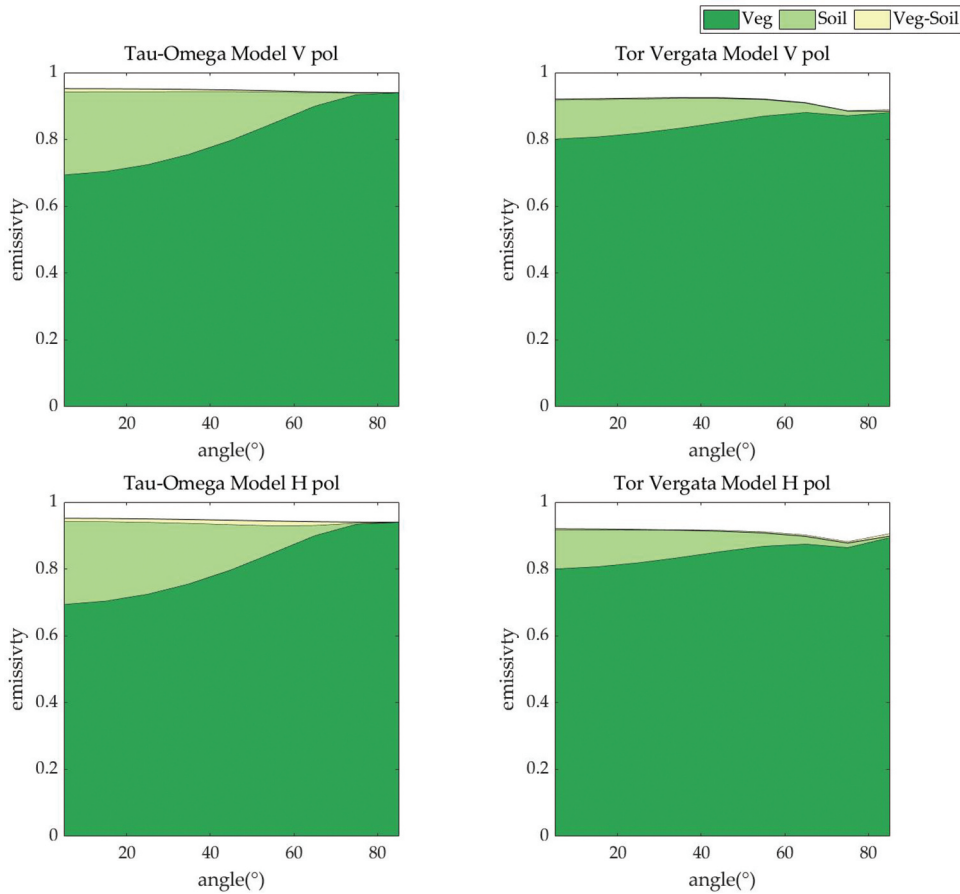
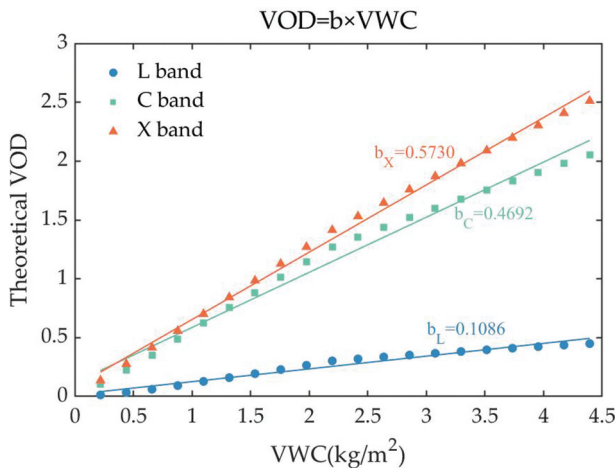


Figure 6. Tau-Omega model and Tor Vergata model brightness temperature composition in the C-band.



**Figure 7.** Tau-Omega model and Tor Vergata model brightness temperature composition in the X-band.



**Figure 8.** The relationship between the VOD calculated by the model and the VWC in the L-b and, C-b and, and X-b and ( $\tau = b \cdot VWC$ ).

approach. Based on the results presented in Figure 9, it can be observed that an increase in vegetation height is positively correlated with an increase in vegetation optical depth. However, when the incidence angle increases, the H and vertical polarizations show different trends. Under vertical polarization, the incidence angle has a greater impact on the vegetation optical depth compared to that under horizontal polarization, in which the difference in the vegetation optical depth caused by

the incidence angle is lower. Additionally, the vegetation optical depth at nadir in the L-band increases with the incidence angle, while in the C-band and X-band, it decreases. The L-band has a longer wavelength and more effective penetration compared to other bands, thus having a significant impact on the transmissivity of the vegetation optical depth at nadir, particularly under a specific biomass. As the angle of incidence increases, the vegetation optical depth also increases. The vegetation optical depth exhibits a significant change from the L-band to the C-band, indicating a strong sensitivity to this transition. However, the sensitivity decreases from the C-band to the X-band. This observation can be attributed to the fact that as the frequency increases, the penetrability of vegetation optical depth remains relatively constant. It further confirms that passive microwaves are more sensitive in the L-band, making it the optimal frequency band for soil moisture retrieval in vegetated areas.

To study the vegetation optical depth during the growth process, the experimental data are chosen to represent corn plants with a planting density of  $0.001 \text{ cm}^{-2}$ .  $C_f$  is calculated after initially solving for  $C_p$  in the solution procedure.

- (1) As specified in Equation (19), the computation of the polarization-dependent parameter,  $C_p$ , is

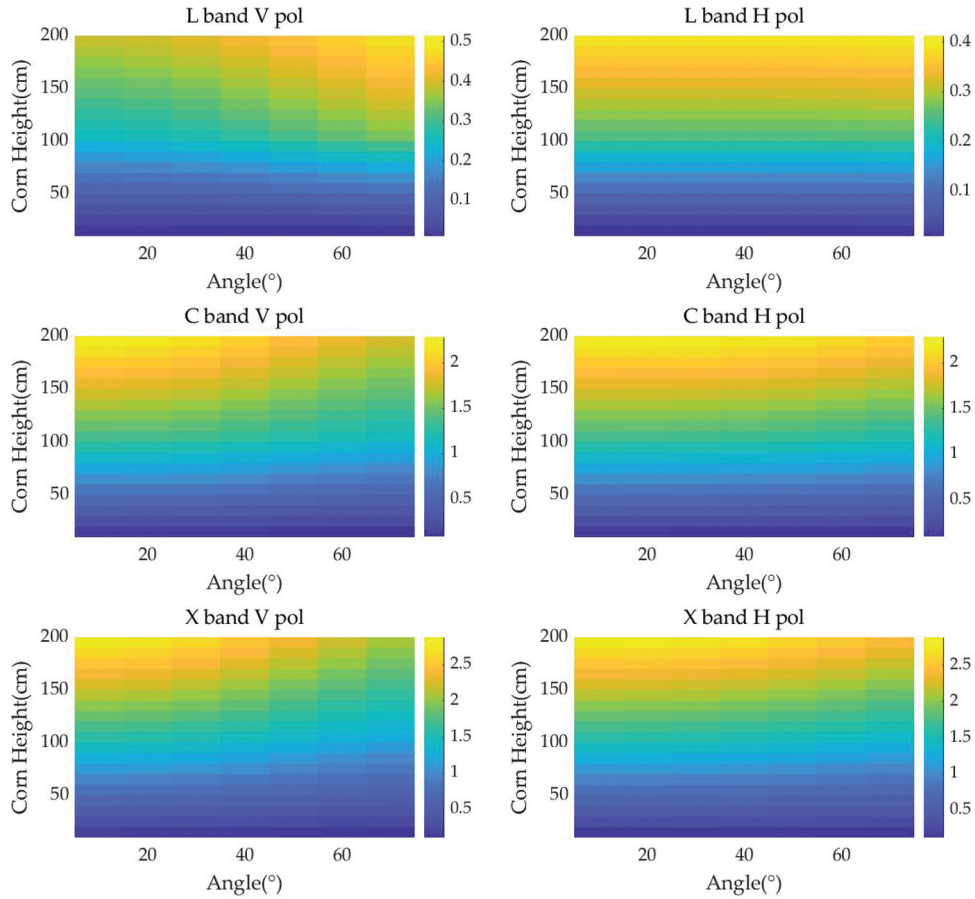


**Figure 9.** Vegetation optical depth with observation angle for different channels.

performed first. The impact of the polarization and frequency components is ignored in favor of the angle as the main factor. The  $C_p$  corresponding to two channels at different angles under the same polarization was computed, as well as the vegetation optical depth at various angles under the same frequency and polarization. The  $C_p$  of dual polarization under the three bands is depicted in the Figure 10. The  $C_p$  of  $0^\circ$  to  $65^\circ$  does not drastically influence after acquiring the abovementioned six distinct channels. As shown in Table 2, the  $C_p$  of six channels is derived by averaging the  $C_p$  of  $0^\circ$  to  $65^\circ$ . Then, Equation (19) can be used to determine the  $\tau_2$  values of various angles within the same band and polarization using  $C_p$ .

- (2) The polarization is considered to be the main factor, and the impacts of the angle and frequency parameters are ignored for the time being. As a result, when considering the polarization dependency of the vegetation optical depth,  $\tau_V = \tau_H = \tau^0$  is obtained under the vertical polarization and horizontal polarization. By meeting this requirement, the  $C_p$  values can be used to calculate two channels with different polarizations and angles.

- (3) The frequency is considered as the main issue, and the effects of the angle and polarization are ignored for the time being. Therefore, to obtain  $C_f$  of the frequency-dependent parameter values of two different frequency channels, we must count  $\tau^0$  under three different polarizations and then insert those values into the analysis equation. Table 3 below displays the  $C_f$  values that were determined by the analysis.

In future studies, the analysis presented here can provide valuable insights into the frequency-dependent and angle polarization-dependent parameters of the vegetation optical depth. The determination of  $C_p$  and  $C_f$  can aid in a more accurate calculation of the VOD for large-scale satellite observations and improved soil moisture retrieval.

### 4.3. Channel dependency of the effective scattering albedo

The effective scattering albedo of corn was calculated using the least square method after fitting the data

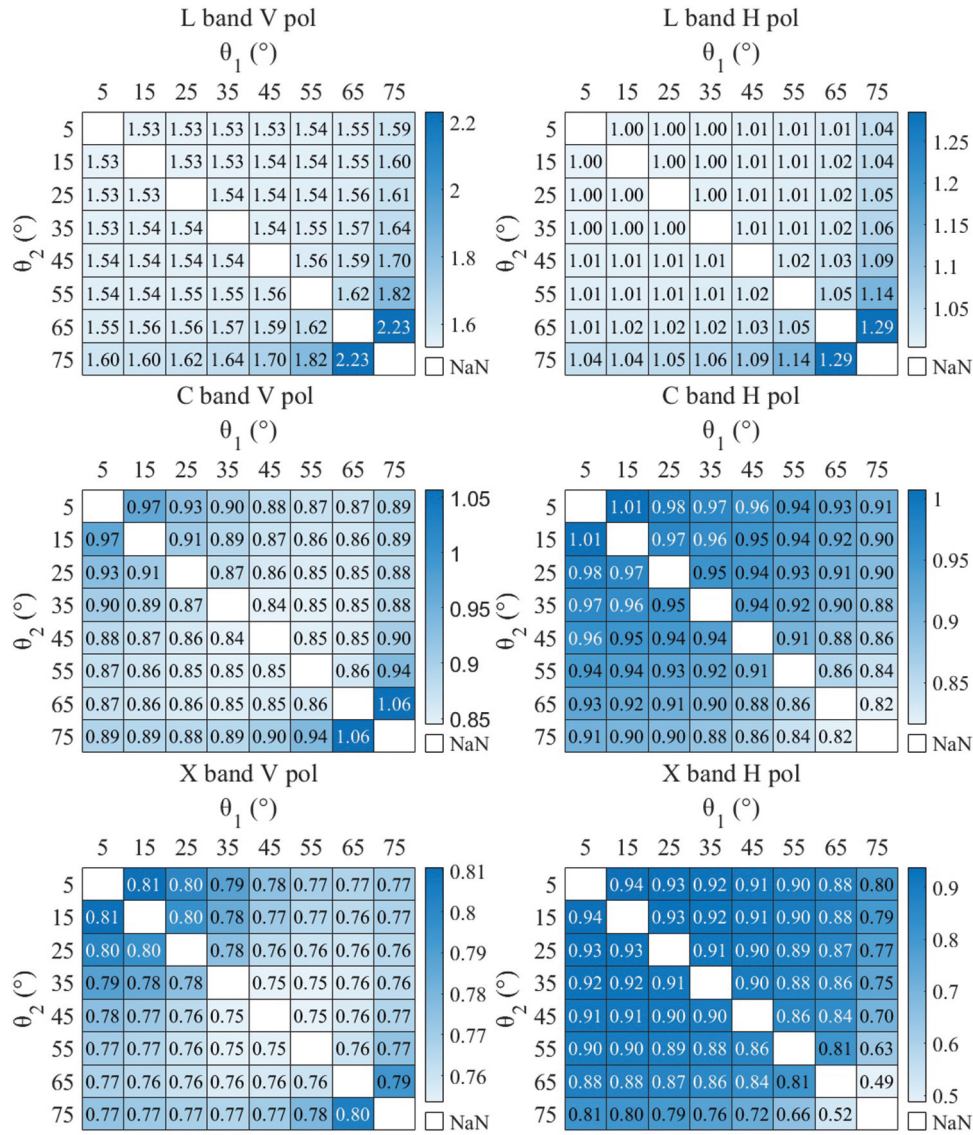


Figure 10. Polarization dependence parameter  $C_p$  at two different angle channels.

Table 2. Polarization dependence parameter ( $C_p$ ) at different channels.

| Frequency        | V Polarization | H Polarization |
|------------------|----------------|----------------|
| L-Band (1.4Ghz)  | 1.5404         | 1.0067         |
| C-Band (6.92Ghz) | .8801          | .9519          |
| X-Band(10.65Ghz) | .7750          | .9070          |

Table 3. The frequency dependence parameter between two different bands.

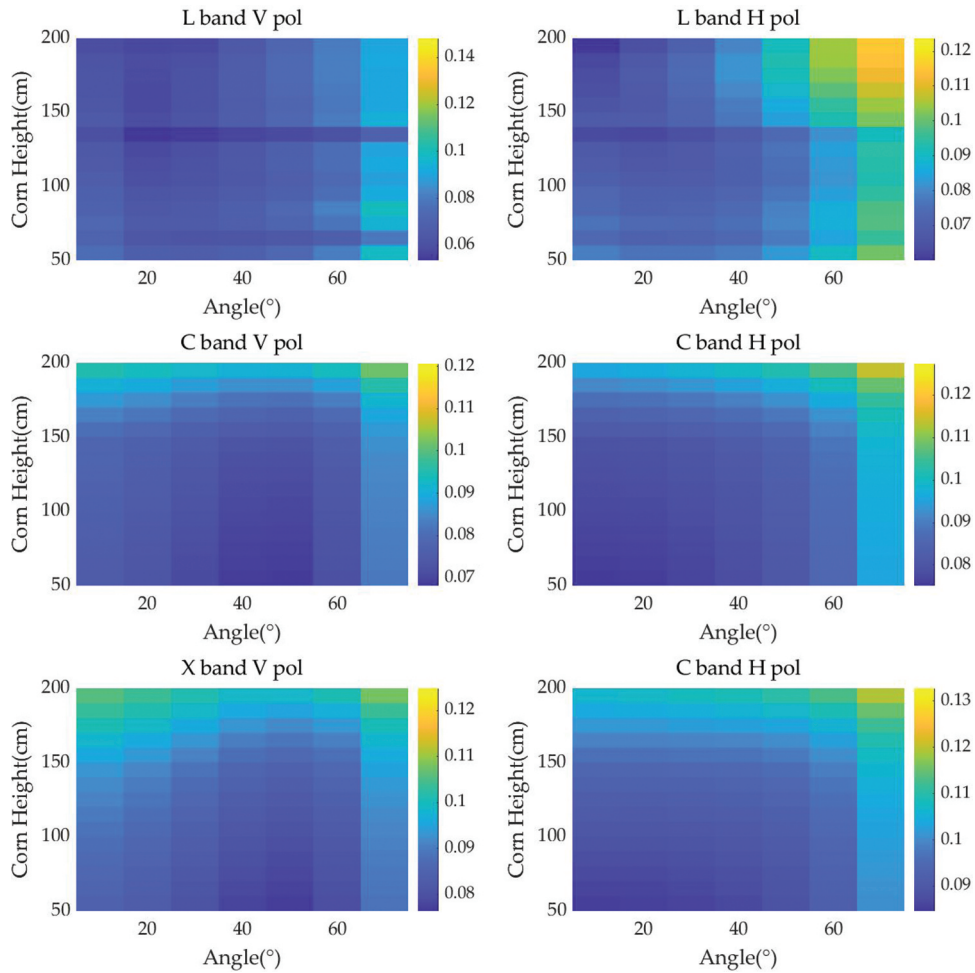
| $f_1$     | $f_2$     | $C_f$  |
|-----------|-----------|--------|
| 1.4 Ghz   | 6.925 Ghz | 0.9154 |
| 1.4 Ghz   | 10.65 Ghz | 0.7978 |
| 6.925 Ghz | 10.65 Ghz | 0.3682 |
| 6.925 Ghz | 1.4 Ghz   | 0.9172 |
| 10.65 Ghz | 1.4 Ghz   | 0.8058 |
| 10.65 Ghz | 6.925 Ghz | 0.3845 |

Table 4. The effective scattering albedo at six channels.

| Frequency        | V Polarization | H Polarization |
|------------------|----------------|----------------|
| L-Band (1.4Ghz)  | .0619          | .0536          |
| C-Band (6.92Ghz) | .0814          | .1025          |
| X-Band(10.65Ghz) | .0888          | .1052          |

simulated by the Tor Vergata model for the emissivity, transmissivity, and ground emissivity to various polarizations and heights across different frequency bands. The results are shown in Figure 11, which displays the effective scattering albedo of corn for the L-band, C-band, and X-band.

After fitting the data simulated by the Tor Vergata model using the least squares method, the effective scattering albedo of corn at different polarizations, heights, and frequency bands was calculated. Figure 11 shows the effective scattering albedo of corn in three frequency bands. The results indicate that the effective scattering albedo of vegetation does not vary significantly with vegetation height or angle. It primarily depends on frequency and polarization, showing an overall increasing trend with increasing frequency. The effective scattering albedo with vertical polarization is slightly higher than that with horizontal polarization at higher frequencies, while both are lower in the L-band. The analysis reveals a more



**Figure 11.** Effective scattering albedo at different angles and different heights.

pronounced variation between the L-band and C-band, whereas as the frequency gradually increases, the multiple scattering effects of microwaves result in smaller changes in the effective scattering albedo, and the sensitivity of the effective scattering albedo to frequency becomes limited. Statistical analysis of the simulated results from the Tor Vergata model demonstrates high fitting accuracy, encompassing all angles and vegetation heights. As show in Table 4, the effective scattering albedo was obtained for six different channels, and the equivalent scattering albedo derived from these six channels can be more easily and accurately applied in the inversion of large-scale zero-order radiative transfer models for satellite observations.

## 5. Conclusions

In this work, the vegetation optical depth and effective scattering albedo of corn crops at different stages of development were estimated through model simulations and their frequency, polarization, and angle dependencies were investigated and discussed. By utilizing the simulated results of the advanced vegetation radiative transfer model (Tor Vergata Model), we can calculate the vegetation optical depth and effective scattering

albedo based on the higher-order radiative transfer model. This approach indeed expands the applicability range of the zero-order model.

The vegetation height is positively correlated with vegetation optical depth. However, when the incidence angle increases, the H and vertical polarizations show different trends. Under vertical polarization, the incidence angle has a greater impact on the vegetation optical depth compared to that under horizontal polarization, in which the difference in the vegetation optical depth caused by the incidence angle is lower. Additionally, the vegetation optical depth at nadir in the L-band increases with the incidence angle, while in the C-band and X-band, it decreases. The analysis of vegetation optical depth determined the polarization dependence parameter ( $C_p$ ) and frequency dependence parameter ( $C_f$ ). The  $C_p$  values for vertical and horizontal polarizations in the L-band were 1.5404 and 1.0067, respectively, while in the C-band, they were 0.8801 and 0.9519, respectively, and in the X-band, they were 0.7750 and 0.9070, respectively. The  $C_p$  values can be used to convert the vegetation optical depth between channels of the same frequency with different angles and polarizations. The frequency

dependence parameter ( $C_f$ ) can convert vegetation optical depth between channels of different frequencies with the same angles and polarizations. The  $C_f$  value between the L- and C-bands was 0.9164, between the L- and X-bands was 0.8018, and between the C- and X-bands was 0.3764. By combining  $C_p$  and  $C_f$  values and incorporating traditional experience in calculating vegetation optical depth, the accuracy of vegetation microwave radiation simulation can be improved. The study concluded the effective scattering albedo in six bands with two polarizations in three adjacent bands, with values of 0.0619 and 0.0536 for vertical and horizontal polarizations in the L-band, 0.0814 and 0.1025 in the C-band, and 0.0888 and 0.1052 in the X-band. Future large-scale satellite observations will greatly benefit from the study of the effective scattering albedo and the computation of the scattering albedo in six channels.

In this paper, we only discussed corn crops. Future research will be expanded to more commonly encountered vegetation-covered areas such as forests, shrubs, and grasslands to better serve large-scale satellite observations and soil moisture retrievals.

## Disclosure statement

No potential conflict of interest was reported by the author(s).

## Funding

This work was jointly supported by National Natural Science Foundation of China (grant number 42090014), National Key Research and Development Program of China (grant number 2021YFB3900104) and the Dragon 5 Cooperation Programme (grant number 59312).

## Notes on contributors

**Jiaqi Zhang** received the B.S. and M.S. from Henan Polytechnic University. His research interests are microwave remote sensing of soil moisture and radiation transfer model.

**Tianjie Zhao** received the B.S. and Ph.D. degrees from Beijing Normal University. He is a Professor with the State Key Laboratory of Remote Sensing Science, Aerospace Information Research Institute, Chinese Academy of Sciences (CAS), Beijing, China. His research interests include microwave remote sensing of soil moisture and its freeze-thaw process.

**Shurun Tan** received the Ph.D. degree in electrical engineering from the University of Michigan. He is currently an Assistant Professor with Zhejiang University/University of Illinois at Urbana-Champaign Institute, International Campus of Zhejiang University. His research interests include EM scattering of random media and periodic

structures, microwave remote sensing, EM information systems with EM wavefunctional devices, EM integrity in high-speed and high-density electronic integration, EM environment, and reliability of complex electronic systems.

**Nemesio J. Rodríguez-Fernández** received the Licentiate degree in fundamental physics and the Ph.D. degree in astrophysics from Universidad Complutense de Madrid, Madrid, Spain, in 1996 and 2002, respectively. Since 2012, he has been a Centre National de la Recherche Scientifique (CNRS) Scientist and a Research Engineer with Centre d'Etudes Spatiales de la Biosphère (CESBIO), Toulouse, France.

**Huazhu Xue** received his PhD in cartography and geographic information systems in the area of quantitative remote sensing from the School of Geography, Beijing Normal University, Beijing, China, in 2012. Since 2012, he has been an associate professor at the School of Surveying and Land Information Engineering, Henan Polytechnic University. His research interests include vegetation parameters inversion, satellite image processing, and GIS applications.

**Na Yang** received her PhD degree from Wuhan University. She was a visiting scientist with the School of Archaeology, Geography and Environmental Science, University of Reading, Reading, UK, in Jun-Nov, 2015. She is currently a lecturer with Henan Polytechnic University, Jiaozuo, China. Her research interests include microwave remote sensing and data assimilation.

**Yann H. Kerr** received the engineering degree from Ecole Nationale Supérieure de l'Aéronautique et de l'Espace, Toulouse, France, the M.Sc. degree in electronics and electrical engineering from Glasgow University, Glasgow, U.K., in 1977, 1981, and the Ph.D. degree in astrophysique géophysique et techniques spatiales from Université Paul Sabatier, Toulouse, France, in 1992. Since 1995, he has been with Centre d'Etudes Spatiales de la Biosphère, Toulouse, France, where he was the Deputy Director from 1995 to 1999 and the Director from 2007 to 2016. His research interests include the theory and techniques for microwave and thermal infrared remote sensing of the Earth, with a focus on hydrology, water resources management, and vegetation monitoring.

**Jiancheng Shi** received the B.A. degree in hydro-geology and engineering-geology from the University of Lanzhou, Lanzhou, China, in 1982, and the M.A. and Ph.D. degrees in geography from the University of California at Santa Barbara (UCSB), Santa Barbara, CA, USA, in 1987 and 1991, respectively. He then worked as a Research Scientist with the Earth Research Institute, UCSB. After 2010, he joined the State Key Laboratory for Remote Sensing Science, Institute of Remote Sensing and Digital Earth, Beijing, China, as the Director. He is currently with the National Space Science Center, Chinese Academy of Sciences, Beijing. He has authored more than 500 journal articles and conference papers that related to the following research topics. He has wide research interests in remote sensing theories and technologies, especially in microwave remote sensing in both active and passive techniques and its applications in water cycle and climatic change, including: 1) microwave modeling of snow, soil, and vegetation properties; especially by using the state-of-the-art theoretical microwave scattering and emission models to develop the simple, fast, and accurate parameterized microwave models



for snow, vegetation, and rough surfaces; 2) development of theory and novel inversion techniques for active and passive microwave remote sensing of soil moisture, snow, and vegetation physical properties; and 3) applications of remote sensing data in water cycle and climatic change studie

## ORCID

Jiaqi Zhang  <http://orcid.org/0009-0009-5222-0826>  
 Tianjie Zhao  <http://orcid.org/0000-0002-0914-599X>  
 Shurun Tan  <http://orcid.org/0000-0002-7331-3484>  
 Nemesio Rodriguez-Fernandez  <http://orcid.org/0000-0003-3796-149X>  
 Huazhu Xue  <http://orcid.org/0000-0003-4046-7935>  
 Na Yang  <http://orcid.org/0000-0003-0923-0681>  
 Yann Kerr  <http://orcid.org/0000-0001-6352-1717>  
 Jiancheng Shi  <http://orcid.org/0000-0002-6163-2912>

## Data availability statement

The data that support the findings of this study are available in National Tibetan Plateau/Third Pole Environment Data Center at <https://doi.org/10.11888/Soil.tpdc.271622>, <https://cstr.cn/18406.11.Soil.tpdc.271622>.

## References

- Anderson, M., C. Neale, F. Li, J. Norman, W. Kustas, H. Jayanthi, and J. Chavez. 2004. "Upscaling Ground Observations of Vegetation Water Content, Canopy Height, and Leaf Area Index During smex02 Using Aircraft and Landsat Imagery." *Remote Sensing of Environment* 92 (4): 447–464. <https://doi.org/10.1016/j.rse.2004.03.019>.
- Bracaglia, M., P. Ferrazzoli, and L. Guerriero. 1995. "A Fully Polarimetric Multiple Scattering Model for Crops." *Remote Sensing of Environment* 54 (3): 170–179. [https://doi.org/10.1016/0034-4257\(95\)00151-4](https://doi.org/10.1016/0034-4257(95)00151-4).
- Byrne, K. A., G. Kiely, and P. Leahy. 2005. "Co2 Fluxes in Adjacent New and Permanent Temperate Grasslands." *Agricultural and Forest Meteorology* 135 (1–4): 82–92. <https://doi.org/10.1016/j.agrformet.2005.10.005>.
- Cheng, X., W. Huang, and J. Gong. 2015. "Adaptive Polarimetric Decomposition Using Incoherent Ground Scattering Models without Reflection Symmetry Assumption." *Geo-Spatial Information Science* 18 (1): 1–10. <https://doi.org/10.1080/10095020.2015.1016201>.
- Dela Torre, D. M. G., J. Gao, and C. Macinnis-Ng. 2021. "Remote Sensing-Based Estimation of Rice Yields Using Various Models: A Critical Review." *Geo-Spatial Information Science* 24 (4): 580–603. <https://doi.org/10.1080/10095020.2021.1936656>.
- Della Vecchia, A., P. Ferrazzoli, L. Guerriero, X. Blaes, P. Defourny, L. Dente, F. Mattia, G. Satalino, T. Strozzi, and U. Wegmuller. 2006. "Influence of Geometrical Factors on Crop Backscattering at C-Band." *IEEE Transactions on Geoscience & Remote Sensing* 44 (4): 778–790. <https://doi.org/10.1109/TGRS.2005.860489>.
- Della Vecchia, A., P. Ferrazzoli, J.-P. Wigneron, and J. P. Grant. 2007. "Modeling Forest Emissivity at L-Band and a Comparison with Multitemporal Measurements." *IEEE Geoscience & Remote Sensing Letters* 4 (4): 508–512. <https://doi.org/10.1109/LGRS.2007.900687>.
- Eom, H. J., and A. Fung. 1984. "A Scatter Model for Vegetation Up to Ku-Band." *Remote Sensing of Environment* 15 (3): 185–200. [https://doi.org/10.1016/0034-4257\(84\)90030-0](https://doi.org/10.1016/0034-4257(84)90030-0).
- Eom, H. J., and A. Fung. 1986. "Scattering from a Random Layer Embedded with Dielectric Needles." *Remote Sensing of Environment* 19 (2): 139–149. [https://doi.org/10.1016/0034-4257\(86\)90067-2](https://doi.org/10.1016/0034-4257(86)90067-2).
- Fernandez-Moran, R., A. Al-Yaari, A. Mialon, A. Mahmoodi, A. A. Bitar, G. D. Lannoy, N. Rodriguez-Fernandez, E. Lopez-Baeza, Y. Kerr, and J.-P. Wigneron. 2017. "Smos-Ic: An Alternative Smos Soil Moisture and Vegetation Optical Depth Product." *Remote Sensing* 9 (5): 457. <https://doi.org/10.3390/rs9050457>.
- Ferrazzoli, P., and L. Guerriero. 1996. "Passive Microwave Remote Sensing of Forests: A Model Investigation." *IEEE Transactions on Geoscience & Remote Sensing* 34 (2): 433–443. <https://doi.org/10.1109/36.485121>.
- Fung, A. K., A. K. Fung, W. R. Baker, R. A. Mantei, H. H. Stein, J. Cohen, and J. L. Barlow. 1994. "Nonpeptide Renin Inhibitors with Good Intraduodenal Bioavailability and Efficacy in Dog." *Journal of Medicinal Chemistry* 37 (19): 2991–3007. <https://doi.org/10.1021/jm00045a003>.
- Gentine, P., J. K. Green, M. Guérin, V. Humphrey, S. I. Seneviratne, Y. Zhang, and S. Zhou. 2019. "Coupling Between the Terrestrial Carbon and Water Cycles—A Review." *Environmental Research Letters* 14 (8): 083003. <https://doi.org/10.1088/1748-9326/ab22d6>.
- Jiang, L., J. Shi, S. Tjuatja, J. Dozier, K. Chen, and L. Zhang. 2007. "A Parameterized Multiple-Scattering Model for Microwave Emission from Dry Snow." *Remote Sensing of Environment* 111 (2–3): 357–366. <https://doi.org/10.1016/j.rse.2007.02.034>.
- Karam, M., and A. Fung. 1988. "Electromagnetic Scattering from a Layer of Finite Length, Randomly Oriented, Dielectric, Circular Cylinders Over a Rough Interface with Application to Vegetation." *International Journal of Remote Sensing* 9 (6): 1109–1134. <https://doi.org/10.1080/01431168808954918>.
- Kerr, Y. H., P. Waldteufel, P. Richaume, J. P. Wigneron, P. Ferrazzoli, A. Mahmoodi, A. A. Bitar, et al. 2012. "The Smos Soil Moisture Retrieval Algorithm." *IEEE Transactions on Geoscience & Remote Sensing* 50 (5): 1384–1403. <https://doi.org/10.1109/TGRS.2012.2184548>.
- Konings, A. G., K. A. Mccoll, M. Piles, and D. Entekhabi. 2015. "How Many Parameters Can Be Maximally Estimated from a Set of Measurements?" *IEEE Geoscience & Remote Sensing Letters* 12 (5): 1081–1085. <https://doi.org/10.1109/LGRS.2014.2381641>.
- Kurum, M. 2013. "Quantifying Scattering Albedo in Microwave Emission of Vegetated Terrain." *Remote Sensing of Environment* 129: 66–74. <https://doi.org/10.1016/j.rse.2012.10.021>.
- Levine, D., R. Meneghini, R. Lang, and S. Seker. 1983. "Scattering from Arbitrarily Oriented Dielectric Disks in the Physical Optics Regime." *JOSA* 73 (10): 1255–1262. <https://doi.org/10.1364/JOSA.73.001255>.
- Mo, T., B. Choudhury, T. Schmugge, J. R. Wang, and T. Jackson. 1982. "A Model for Microwave Emission from Vegetation-Covered Fields." *Journal of Geophysical Research: Oceans* 87 (C13): 11229–11237. <https://doi.org/10.1029/JC087iC13p11229>.
- Monsivais-Huertero, A., and J. Judge. 2010. "Comparison of Backscattering Models at L-Band for Growing Corn." *IEEE Geoscience & Remote Sensing Letters* 8 (1): 24–28. <https://doi.org/10.1109/LGRS.2010.2050459>.

- Monsivais-Huertero, A., P.-W. Liu, and J. Judge. 2018. "Phenology-Based Backscattering Model for Corn at L-Band." *IEEE Transactions on Geoscience & Remote Sensing* 56 (9): 4989–5005. <https://doi.org/10.1109/TGRS.2018.2803153>.
- Natsagdorj, E., T. Renchin, M. Kappas, B. Tseveen, C. Dari, O. Tsend, and U.-O. Duger. 2017. "An Integrated Methodology for Soil Moisture Analysis Using Multispectral Data in Mongolia." *Geo-Spatial Information Science* 20 (1): 46–55. <https://doi.org/10.1080/10095020.2017.1307666>.
- Osborn, J. A. 1945. "Demagnetizing Factors of the General Ellipsoid." *Physical Review* 67 (11–12): 351. <https://doi.org/10.1103/PhysRev.67.351>.
- Pampaloni, P., and S. Paloscia. 1986. "Microwave Emission and Plant Water Content: A Comparison Between Field Measurements and Theory." *IEEE Transactions on Geoscience & Remote Sensing* 6 (6): 900–905. <https://doi.org/10.1109/TGRS.1986.289705>.
- Park, C.-H., T. Jagdhuber, A. Colliander, J. Lee, A. Berg, M. Cosh, S.-B. Kim, Y. Kim, and V. Wulfmeyer. 2020. "Parameterization of Vegetation Scattering Albedo in the Tau-Omega Model for Soil Moisture Retrieval on Croplands." *Remote Sensing* 12 (18): 2939. <https://doi.org/10.3390/rs12182939>.
- Stiles, J. M., K. Sarabandi, and F. T. Ulaby. 2000. "Electromagnetic Scattering from Grassland. Ii. Measurement and Modeling Results." *IEEE Transactions on Geoscience & Remote Sensing* 38 (1): 349–356. <https://doi.org/10.1109/36.823930>.
- Talebiesfandarani, S., T. Zhao, J. Shi, P. Ferrazzoli, J.-P. Wigneron, M. Zamani, and P. Pani. 2019. "Microwave Vegetation Index from Multi-Angular Observations and Its Application in Vegetation Properties Retrieval: Theoretical Modelling." *Remote Sensing* 11 (6): 730. <https://doi.org/10.3390/rs11060730>.
- Ulaby, F. T., R. K. Moore, and A. K. Fung. 1982. *Microwave Remote Sensing: Active and Passive: Volume 2—Radar Remote Sensing and Surface Scattering and Emission Theory*. Reading, MA: Addison-Wesley.
- Wigneron, J.-P., J.-C. Calvet, T. Pellarin, A. A. Van De Griend, M. Berger, and P. Ferrazzoli. 2003. "Retrieving Near-Surface Soil Moisture from Microwave Radiometric Observations: Current Status and Future Plans." *Remote Sensing of Environment* 85 (4): 489–506. [https://doi.org/10.1016/S0034-4257\(03\)00051-8](https://doi.org/10.1016/S0034-4257(03)00051-8).
- Wigneron, J.-P., M. Pardé, P. Waldteufel, A. Chanzy, Y. Kerr, S. Schmidl, and N. Skou. 2004. "Characterizing the Dependence of Vegetation Model Parameters on Crop Structure, Incidence Angle, and Polarization at L-Band." *IEEE Transactions on Geoscience & Remote Sensing* 42 (2): 416–425. <https://doi.org/10.1109/TGRS.2003.817976>.
- Zhang, Z., X. Yu, S. Zhao, and L. Chai. 2014. "Assessment and Analysis of Microwave Emissivity and Transmissivity of a Deciduous Forest Towards the Estimate of Vegetation Biomass." *Science China Earth Sciences* 57 (3): 534–541. <https://doi.org/10.1007/s11430-013-4698-y>.
- Zhao, T., L. Hu, S. Li, D. Fan, P. Wang, D. Geng, and J. Shi. 2021. "Multi-Frequency and Multi-Angular Ground-Based Microwave Radiometer and Surface Parameters Experimental Data for Cropland in 2017, National Tibetan Plateau Data."
- Zhao, T., L. Hu, J. Shi, H. Lü, S. Li, D. Fan, P. Wang, D. Geng, C. S. Kang, and Z. Zhang. 2020. "Soil Moisture Retrievals Using L-Band Radiometry from Variable Angular Ground-Based and Airborne Observations." *Remote Sensing of Environment* 248: 111958. <https://doi.org/10.1016/j.rse.2020.111958>.
- Zhao, T., J. Shi, D. Entekhabi, T. J. Jackson, L. Hu, Z. Peng, P. Yao, S. Li, and C. S. Kang. 2021. "Retrievals of Soil Moisture and Vegetation Optical Depth Using a Multi-Channel Collaborative Algorithm." *Remote Sensing of Environment* 257:112321. <https://doi.org/10.1016/j.rse.2021.112321>.
- Zhao, T., J. Shi, L. Lv, H. Xu, D. Chen, Q. Cui, T. J. Jackson, G. Yan, L. Jia, and L. Chen. 2020. "Soil Moisture Experiment in the Luan River Supporting New Satellite Mission Opportunities." *Remote Sensing of Environment* 240: 111680. <https://doi.org/10.1016/j.rse.2020.111680>.